



Published in final edited form as:

J Biomater Sci Polym Ed. 2013 ; 24(9): 1041–1056. doi:10.1080/09205063.2012.735097.

Synthesis of Macroporous Poly(dimethylsiloxane) Scaffolds for Tissue Engineering Applications

Eileen Pedraza^{a,b}, Ann-Christina Brady^{b,c}, Christopher A. Fraker^{a,b,c}, and Cherie L. Stabler^{a,b,c}

^aDepartment of Biomedical Engineering, College of Engineering, University of Miami, Coral Gables, FL 33134 USA

^bDiabetes Research Institute, Leonard M. Miller School of Medicine, University of Miami, Miami, FL 33136 USA

^cDeWitt Daughtry Department of Surgery, Leonard M. Miller School of Medicine, University of Miami, Miami, FL 33136 USA

Abstract

Macroporous, biostable scaffolds with controlled porous architecture were prepared from poly(dimethylsiloxane) (PDMS) using sodium chloride particles (NaCl) and a solvent casting and particulate leaching (SCPL) technique. The effect of particulate size range and overall porosity on the resulting structure was evaluated. Results found 90% v/v scaffolds and particulate ranges above 100 μm to have the most optimal open framework and porosity. Resulting hydrophobic PDMS scaffolds were coated with fibronectin and evaluated as a platform for adherent cell culture using human mesenchymal stem cells. Biocompatibility of PDMS scaffolds was also evaluated in a rodent model, where implants were found to be highly biocompatible and biostable, with positive extracellular matrix deposition throughout the scaffold. These results demonstrate the suitability of macroporous PDMS scaffolds for tissue engineering applications where strong integration with the host is desired.

Keywords

matrix; macroporous; poly(dimethylsiloxane); cellular transplantation; mesenchymal stem cells; biocompatibility

1. Introduction

The field of tissue engineering has great potential to treat and/or cure numerous afflictions, from heart damage to cartilage degradation to organ replacement. Three-dimensional scaffolds for tissue engineering play a critical role in providing a three-dimensional structure and mechanical integrity to the implant, as well supporting cell adhesion, distribution, and proliferation. Optimal integration of the scaffold into the host requires constructs to retain a high surface area to volume ratio for: optimal cell-polymer interactions, space for host and

transplant remodeling, extracellular matrix (ECM) deposition, intra-device vascularization, reduced host inflammation, and minimal diffusional impedance.[1–4] Ideally, the overall porosity should be at least 90%, with interconnected pores > 100 μm in diameter, e.g. macroporous.[5, 6]

The selection of an appropriate biocompatible material and fabrication method that meets the above outlined criteria is a complicated task. Material selection is tissue-specific and requires a balance of the desired properties of the implant, such as mechanical integrity, pore structure, immunogenicity, biostability, and biorecognition. Synthetic materials, such as poly(ϵ -caprolactone) (PCL), poly(ethylene glycol) (PEG), and poly(α -hydroxy esters) like poly(glycolic acid) (PGA), poly(lactic acid) (PLA), and poly(lactic-*co*-glycolic acid) (PLGA), are commonly used for tissue engineering scaffolds.[7–10] PGA and PLGA have been particularly prevalent in the design of macroporous scaffolds, given their ease in fabrication.[11–13] Their high degradability, however, might not always be desirable, particularly when their degradation products have the potential to invoke an inflammatory response.[8, 14] In many tissue engineering applications, biostability and retrievability are highly desirable traits, e.g. implantable glucose sensors[15], vascular substitutes[16], articular cartilage replacements[17], and islet transplantation[18]. Thus, the engineering of macroporous scaffolds with high biocompatibility and biostability could have broad applications. With this goal in mind, we selected the polymer poly(dimethylsiloxane) (PDMS). PDMS is an excellent candidate for long term implantation, due to its demonstrated high degree of biocompatibility and biostability following clinical implantation.[19–25] In addition, given the oxygen demand of cells, the high solubility of oxygen in PDMS renders it an ideal material for cell-based implants.[26–28] While generally hydrophobic, the PDMS surface can be easily modified, via adsorption of proteins, plasma oxygenation, or conjugation of RGD peptides, to create surfaces that promote cellular adhesion and biorecognition.[29–35] Furthermore, the hydrophobic nature of PDMS permits the encapsulation of compounds for slow release into the scaffold microenvironment. In this manner, the scaffold can be used as a platform for drug delivery, if doped with immunosuppressant compounds or with hydrolytically reactive agents for oxygen delivery.[36, 37] Due to these desirable traits, PDMS is a material with a long history in medical implantation with multiple forms generated for various tissue engineering applications [31, 32, 38, 39]. The fabrication of macroporous PDMS scaffolds with the desired features of high porosity, strong pore interconnectivity, and larger porosity (> 100 μm) has not, to our knowledge, been explored.

In this study, we fabricated PDMS macroporous scaffolds using the solvent casting and particulate leaching technique (SCPL). The advantage of SCPL is that it does not involve hazardous solvents and is straightforward: the degree of porosity can be controlled by varying the percent of particulate to solvent, and the pore size is dictated by the diameter of the porogen. We demonstrate that macroporous PDMS scaffolds can be fabricated with a large surface to volume ratio and controllable porosity, while maintaining structural integrity and interconnectivity. The ability to modify the hydrophobic surface of the scaffold was evaluated by coating with an adhesion protein and subsequent culture of human mesenchymal stem cells. Furthermore, the endotoxin content and *in vivo* biocompatibility of

the scaffold was examined. The implications of this platform for tissue engineering applications are discussed.

2. Materials and Methods

2.1 Materials

The silicone polymer components were purchased from GE Silicone (RTV 615). Sodium chloride crystals were purchased from Mallinckrodt Baker (Center Valley, PA). Sieves with openings of 53 μm , 106 μm , 150 μm , 250 μm , 425 μm , and 600 μm were purchased from W.S. Tyler (Mentor, OH) through VWR (Radnor, PA). Human plasma fibronectin (FN) was purchased from Gibco (Grand Island, NY). Biotin conjugated fibronectin antibody was purchased from Rockland Immunochemicals (Gilbertsville, PA) and streptavidin-FITC was purchased from Sigma-Aldrich (St. Louis, MO). All culture media was purchased from Mediatech (Manassas, VA). MTT assay was purchased from Promega (Madison, WI). LIVE/DEAD Viability/Cytotoxicity Assay Kit and CAS block were purchased from Invitrogen (Grand Island, NY). Insulin ELISA was purchased from Mercodia (Winston Salem, NC). Chromogenic kinetic limulus amebocyte lysate (LAL) assay was purchased from Lonza (Switzerland).

2.2 Scaffold Fabrication

Macroporous PDMS scaffolds were fabricated using the solvent casting and particulate leaching technique (SCPL), with sodium chloride (NaCl) crystals as the particulate and poly(dimethylsiloxane) (PDMS) as the solvent. Pore size and degree of porosity were individually optimized by varying the particle size and polymer to particle ratio, respectively. The salt was dried for at least 24 hrs and stored at 40 °C in a drying oven to remove residual air moisture. It was sifted through sieves of varying mesh sizes in order to obtain a specific range of salt diameters: 53 to 106 μm , 150 to 250 μm , 250 to 425 μm , and 425 to 600 μm . The density of the silicone polymer components and the salt for each size range was determined by weight and volume measurements. Scaffolds were fabricated with varying expected porosities: 85%, 90%, 95%, and 97%, based on the volumetric percentage of salt to total volume of scaffold. The silicone polymer was prepared by combining PDMS monomer with platinum catalyst, 4:1 v/v. The desired volume of salt was measured (based on density calculations) and thoroughly mixed into the PDMS. The salt/silicone mixture was loaded into prefabricated, PDMS based molds (10 mm diameter, 2 mm height), compressed using 20 g weight, and incubated at 37 °C for 48 hrs to permit crosslinking of the silicone. The salt was leached from the scaffolds by immersion in deionized water for 72 hrs, with exchange of water every 24 hrs. To demonstrate complete dissolution of salt, scaffolds were sectioned 24, 48, and 72 hrs after salt leaching and imaged by SEM for absence of salt crystals. Afterwards, the scaffolds were dried in an oven at 40 °C for 24 hrs and steam sterilized in an autoclave.

Scaffold design parameters were optimized by assessing scaffolds of varying pore sizes and intended porosities for differences in structural stability, porosity, and particle retention. Degree of porosity was optimized by fabricating scaffolds of equal pore size (250 to 425 μm), but varying intended porosities (85%, 90%, 95%, and 97%). They were examined for

structural stability by visual inspection, scanning electron microscopy (SEM) imaging, and porosity measurements. Next, pore size was optimized by fabricating scaffolds with the equal porosity (based on the preceding study's results) but varying pore sizes (53 to 106 μm , 150 to 250 μm , 250 to 425 μm , and 425 to 600 μm). Their porous structure was examined by SEM imaging and porosity measurements.

2.3 Morphological Characterization of Scaffolds

Scanning electron microscopy (SEM) (JEOL, JSM-5600LV, 29 Pa, 20 kV) was employed to visualize surface roughness, pore size, degree of porosity, and tortuosity of the scaffold for varying porosities and pore sizes. To enhance our ability to visualize the scaffold surface, sputter coating was circumvented by acquiring images using back-scatter. Image analysis using Metamorph software (Molecular Devices) was performed on SEM images to determine average pore size and interconnectivity of pores. For all images, pixel size was calibrated to physical dimensions. The width and length dimensions of the pore size within a set field of view were recorded and averaged (at least 15 pores per scaffold). Interconnectivity was assessed by quantifying the number of interconnected pores relative to non-connected or blocked pores. Measurements were taken for 5 images per scaffold (at 50 \times magnification). Total porosity (interconnected and non-connected pores) of the scaffold was quantified by gross measurements and weights. The dry weight (m_{silicone}) and wet weight ($m_w + m_{\text{silicone}}$), following soaking in ddH₂O, of scaffolds was recorded. Porosity was calculated using known densities of water and silicone (ρ_w and ρ_{silicone}), by applying it to Equation 1.

$$\text{porosity} = \frac{m_w / \rho_w}{\left(m_w / \rho_w + m_{\text{silicone}} / \rho_{\text{silicone}} \right)} \quad (1)$$

2.4 Surface Modification

In selected studies, the scaffold surface was coated with human plasma fibronectin (FN) by incubating the scaffold in a 250 $\mu\text{g}/\text{mL}$ FN solution in water for 24 hrs. Surface coating of proteins for FN coated scaffolds was visualized via confocal microscopy. First, unbound FN was washed from the coated scaffolds using deionized water (two 1 mL washes, 2 min each), followed by incubation of the scaffolds in CAS block for 24 hrs. Scaffolds were incubated with 10 $\mu\text{g}/\text{mL}$ of biotin conjugated anti-fibronectin for 1 hr, and subsequently incubated in 10 $\mu\text{g}/\text{mL}$ of Streptavidin-FITC for 30 min. Following labeling, scaffolds were washed in PBS. The uniformity of the FN coated scaffold surface was visualized through confocal imaging (Zeiss LSM 510) and compared to controls: noncoated scaffolds treated with both primary and secondary antibodies; and FN coated scaffold treated only with secondary antibody, but no primary.

2.5 Cell Isolation, Culture, and Loading on Scaffolds

Human mesenchymal stem cells (MSC), isolated from human umbilical cord blood, were kindly donated by Dr. Luca Inverardi at passage 3. Prior to seeding on scaffolds, MSCs were

cultured as monolayers in α -minimum essential medium (α -MEM; Gibco) supplemented with fetal bovine serum (FBS; Gibco) in a humidified 37°C, 5% CO₂/ 95% air incubator. All MSC experiments were conducted between passages 4–6. The cells were harvested from monolayers via 0.25% (w/v) trypsin–EDTA (Gibco) and counted via trypan blue. MSCs were seeded onto either noncoated or fibronectin coated PDMS scaffolds at a loading density of 3×10^5 cells per scaffold in 50 μ L of media and incubated for 30 min prior to the addition of 4 mL of media for long term culture. Media was exchanged every 2–3 days following MSC loading.

2.6 Endotoxin Evaluation

Following fabrication and sterilization, endotoxin levels within noncoated and fibronectin coated scaffolds were quantified by chromogenic kinetic limulus amoebocyte lysate (LAL) assay (Lonza, MD). The assay was performed on both the eluent from the scaffold and on the scaffold itself to detect any persistently adherent endotoxins. Eluent was obtained following incubation of 3 scaffolds in 1 mL deionized water for 24 hr. Endotoxin presence on the scaffold surface was evaluated via incubation with the enzyme and monitoring changes in optical density at 405 nm for 1 hour. Results were compared to a calibration curve of endotoxin standards (range 0.005 – 5 EU/mL) and dH₂O only controls.

2.7 Biocompatibility of Scaffold

In vivo biocompatibility of the silicone scaffold was assessed via subcutaneous implantation of PDMS scaffolds (90% v/v and 250–425 μ m pore size; 5 mm diameter; 2 mm thickness) into 1 cm subcutaneous pockets in the abdomen of Lewis rats. All procedures were conducted according to the guidelines of the Committee on Care and Use of Laboratory Animals, Institute of Laboratory Animal Resources (National Research Council, Washington DC) and approved by the University of Miami. Implants were explanted on days 3, 14, and 30, fixed in formalin, and sliced into 5 μ m cross-sections. Histological analysis performed included hematoxylin and eosin (H&E) and Masson's trichrome stain. To provide context of the silicone scaffold on the biocompatibility spectrum for this site, results for PDMS scaffold, uncoated or coated with fibronectin, were compared to a negative control (no material implanted, surgery only) to a positive control (Dacron fibrous mats). Dacron was selected as the positive control, given its established poor biocompatibility when compared to other biostable materials[40]. Dacron mats were generously donated by Innovia (Miami, FL). All materials were treated with extensive washes in ultrafiltered water and autoclaved prior to implantation.

Grading of host response to material was performed via a scoring system, which ranked the presence of giant cells and/or macrophages, degree of lymphocytic infiltrate, and degree of fibrosis. Giant cell and/or macrophage presence was graded as follows: no cells (0); scattered cells (1); numerous cells at focal interfaces of the material (2); or numerous cells surrounding the material (3). The degree of lymphocytic infiltrate was graded: no visible infiltrate (0); minor infiltrate (2); moderate infiltrate (2); or extensive infiltrate (3). The degree of fibrosis was scaled: none (0); 1–2 cell layers (1); 3 to 5 cell layers (2); or greater than 5 cell layers thick (3). The total biocompatibility score was derived from the summation of these three factors, with higher scores indicating a larger inflammatory response. For each

implant, two separate histological slides (2 sections per slide) were assessed via inspection of multiple areas within the slide. Histological slides were independently graded by three reviewers, which gave a single score for each parameter. Infiltration of host tissue into the material for noncoated versus fibronectin coated PDMS scaffolds was evaluated via two dimensional Metamorph analysis, where trichrome stained histological samples were assessed. The entire trichrome stained slide was scanned using PathScan to image the entire cross-section of the implant area. The periphery of the scaffold was highlighted as the area of interest (AOI). Positive staining within the AOI (excluding scaffold itself) was then quantified by setting a color threshold to mark all stained areas and expressed as the percentage of the total AOI area to determine percentage of infiltration area. Three independent cross-sections were quantified per group.

2.8 Statistical Analysis

The number of replicates is indicated in the figure legends, and results are expressed as mean \pm SD. Statistical analysis was performed on all samples using ANOVA, with Tukey's multiple comparison test to evaluate difference between groups. Differences were considered significant when $p < 0.05$.

3. Results and Discussion

3.1 Fabrication and Characterization of PDMS Scaffolds

In this study, we sought to fabricate a highly porous scaffold capable of providing spatial distribution for implanted cells, mechanical support, and full retrievability. Macroporous PDMS scaffolds (10 mm diameter, 2 mm thickness) were fabricated and assessed for optimal porosity and pore size. Optimal porosity was investigated by examining scaffolds of 250 to 425 μm pore size and varying overall porosity from 85 to 97 % vol. NaCl / vol. PDMS. Scaffolds were evaluated via visual inspection of mechanical integrity, scanning electron microscopy, and porosity measurements. The effect of overall porosity on the scaffold properties is summarized in Table 1.

Visually, 85 % and 90 % porous scaffolds typically retained their original dimensions (10 mm diameter; 2 mm height; $50\pi \text{ mm}^3$), although scaffolds tended to expand following salt leaching, as a consequence of water influx increasing the pressure within the scaffold pore. Scaffolds of 95 % and 97 % overall porosity, shrank significantly to 22 and 13 % of their original size, respectively (Table 1). This is likely due to the high void volume and the tensile strength of the PDMS, which weakens the scaffold structure causing it to collapse on itself. Figure 1 shows representative photographs and SEM images of 85, 90, and 95 % scaffolds, at low and high magnification for comparison. Images illustrate strong interconnectivity of pores for all scaffolds; however, at 95 % overall porosity, scaffolds clearly exhibit collapse and distortion of the pores. Pore size measurements, calculated via SEM images, summarize these observations, with a significant decrease in the measured pore size ranges when overall porosity was greater than 90 %. Calculations of porosity from gross measurements and weights ($n = 3$ per group) found that scaffolds made from 85, 90, 95, and 97 % vol. NaCl / vol. PDMS were found to have an actual measured porosity of 83, 85, 79, and 73 %, respectively (Table 1). This further supports SEM and pore size

measurements, whereby scaffolds at 85 and 90 % porosity were of comparable porosity and pore inter-connectivity, while scaffolds higher than 90 % exhibited a collapse of pore structure. Scaffolds with 90 % porosity achieved the best compromise between low bulk material volume, pore interconnectivity, and high mechanical stability and were used for all subsequent studies.

The pore size of a scaffold is of critical importance, given that adequate vascularization of the scaffold is vital for implant integration. The pore size should be large enough to accommodate incoming blood vessels, as well as to facilitate complete host integration and remodeling. The effect of salt particulate size on the final pore size of the scaffold was examined for 90 % vol NaCl / vol PDMS porous scaffolds by varying the salt diameter within the following ranges: 53 to 106 μm , 150 to 250 μm , 250 to 425 μm , and 425 to 600 μm . The structure of PDMS scaffolds was evaluated by SEM and wet / dry weight measurements. As shown in Figure 2 and summarized in Table 2, PDMS scaffolds were highly porous, with pore sizes representative of the salt crystal diameter. Moreover, the pores appear interconnected and tortuous, where pore interconnectivity positively correlated to the average pore size, i.e. the greater the pore size, the greater the interconnectivity, as summarized in Table 2. For all particulate ranges tested except from 53 to 106 μm , resulting scaffolds were mechanically sound and maintained their original shape and dimension. Significant reduction of the overall scaffold dimensions were observed for scaffolds fabricated using 53 to 106 μm NaCl particulate sizes, as illustrated in Figure 2. Gross measurements and weights (n=3) found that 53 to 106 μm pore size scaffolds had an actual porosity of 73 %, while the rest of the scaffolds had an actual porosity of 85 % porosity (± 5 %). Therefore, with the exception of the smallest particulate size measured, the overall porosity of the scaffold did not vary depending on pore size. Overall, at 90 % v/v porosity, pore size ranges above ~ 100 μm provide desirable properties of open pores, pore interconnectivity, and appropriate overall porosity. The selection of optimal pore size range can vary depending on the particular application of the scaffold. The PDMS surface is not as smooth as desired; the edges are rough and there is extraneous flack. Thus, future studies are focused on decreasing the surface roughness of the PDMS through the use of smooth particulates and greater mold compression during SCPL fabrication.

Since the native PDMS surface is hydrophobic, modification is necessary if cell adherence during *in vitro* culture is desired. Surface modification of the PDMS scaffolds with fibronectin (FN) was achieved via overnight incubation with 250 $\mu\text{g}/\text{mL}$ fibronectin solution. Following incubation and washing, the surface characteristics of the hydrophobic material were observationally different, with ease in hydration of inner scaffold region following protein coating. The presence of the FN coating on scaffolds was evaluated through confocal imaging of fluorescent antibody stains. Figure 3 illustrates a uniform fluorescence throughout the surface and within the inner pore surfaces of PDMS scaffolds incubated with fibronectin, indicating a uniform coating of the fibronectin on the scaffold surface. Positive fluorescent staining was absent for noncoated scaffolds. Alternatively, adsorption of albumin and serum proteins was also achieved via overnight incubation (data not shown). This indicates that the silicone scaffold surface can be easily modified with various protein coatings to encourage cellular attachment. More elegant methods for surface

medication are feasible; with published methods illustrating the use of plasma oxygenation for simple surface conjugation to create surfaces that promote cellular adhesion.[29–35]

3.2 Cell adherence and proliferation on scaffold

The effects of surface modification on the attachment and proliferation of adherent cells was investigated through the use of human mesenchymal stem cells (hMSC) cultured on either noncoated or fibronectin coated scaffolds. Proliferation and viability of cells was evaluated 2 and 7 days after loading using LIVE/DEAD assay and confocal microscopy. As Figure 4 illustrates, cellular adhesion on the noncoated scaffolds was minimal, with rounded, non-adherent cells observed on days 2 and 7, and no observable increase in cell number. Conversely, for fibronectin coated scaffolds, hMSC adopted a stretched, adherent morphology. An increase in viable hMSC cell presence was observed between day 2 and 7, indicating proliferation of the MSCs on the scaffold. Additional measurements of MSC proliferation were performed via metabolic assay MTT, which found significant increases in cell number over the course of the seven day culture period (data not shown). While nonspecific adsorption of proteins during media incubation likely induces protein fouling of the PDMS surface over time[41], this data highlights the importance of pre-treating the PDMS surface with proteins prior to cell culture for optimal cellular adhesion and proliferation.

3.3 Biocompatibility of Scaffold

The endotoxin level of the scaffold was assessed to minimize the potential to induce a pyrogenic response to the PDMS scaffold when implanted. Endotoxin levels were below 0.05 EU/mL for both noncoated and fibronectin coated scaffolds (values fell within the range of 0.005 EU/mL to 0.05 EU/mL for the n = 3 scaffolds tested for each group).

While silicone is known for its high biocompatibility and biostability,[35, 42–44] we sought to evaluate the host response to these PDMS scaffolds. PDMS scaffolds, with or without fibronectin coating, were implanted in the subcutaneous space in Lewis rats and explanted on days 7, 14, and 30. Explanted PDMS scaffolds were compared to Dacron (positive control) and absence of material (negative control) by hematoxylin & eosin (H&E) and Masson's trichrome staining. H&E permits visualization of cellular presence, whereas trichrome identifies collagen deposition (blue) and elastin or fibrous deposition (red). Histological assessment found strong biocompatibility, host integration, and biostability of the PDMS scaffolds. As shown in Figure 5, histological cross-sections of explanted implants found silicone to be superior to Dacron material, with positive remodeling and matrix deposition within pores, as well as the absence of significant fibrotic tissue. Minimum fibrosis was observed in the PDMS scaffold explants, even on day 30. Macrophages and giant cells were present within the scaffold after 14 days *in vivo*. This presence was still observed on day 30. After 30 days, however, no degradation or infiltration within the PDMS material itself was observed, indicating high biostability of the PDMS scaffolds. Overall biocompatibility of the implants was scored for all time points. At days 3 and 14, all biomaterial implants scored significantly higher than the negative control implants (no material). By day 30, however, both the PDMS scaffold noncoated and fibronectin coated implants scored at a level statistically identical to the negative controls (no material),

illustrating resolution of the host response to the material (Figure 6). Dacron scored significantly higher than fibronectin coated PDMS scaffolds and the control groups on all time points, and higher than noncoated PDMS scaffolds on day 30. As Figure 7 illustrates, multiple blood vessels were observed infiltrating deep within the PDMS scaffolds on days 14 and 30. Cellular and vascular infiltration into scaffold indicates that the macroporosity of the implants permits the infiltration of host cells and vasculature. Metamorph quantification of overall cellular infiltration and extra-cellular matrix deposition (Figure 8) found significant increases in remodeling and cellular infiltration within the scaffold during the first two weeks of implantation ($p < 0.001$), with a plateau by day 14 ($p > 0.05$ from day 14 to day 30); however, no statistical difference between the noncoated and fibronectin coated scaffolds was observed ($p = 0.2857$). This is likely due to adsorption of proteins onto the PDMS surface following implantation.[45–47]

As a scaffold, PDMS was found to be highly stable, with no visual signs of degradation during the 30 days test period. The inflammatory response to the scaffold was minimal, with the absence of fibrosis. While foreign body giant cells were observed in areas of the scaffold, this is likely instigated by surface defects and roughness of the final PDMS scaffold. Future designs seek to minimize this response, as outlined previously. Overall, the favorable results of the biocompatibility and endotoxin tests demonstrate that PDMS scaffolds are suitable for application *in vivo*.

Moreover, the scaffold has the potential to serve as a platform for further modulating the local environment. The nature of PDMS is one where materials may be easily incorporated within the matrix for slow release. Of particular interest is the incorporation of hydrophobic drugs, which may then release in a controllable manner over time.[48–50] By applying this technique to the scaffold, a new material can be created that provides a microniche for the cellular implant. Future studies are evaluating the potential of this PDMS-based macroporous platform to deliver beneficial agents, including anti-inflammatory and/or immunomodulatory agents and oxygen to the localized islet transplant environment.[36, 37]

4. Conclusion

Biocompatible, PDMS scaffolds were successfully fabricated with intended porosities and a controllable pore size range. Optimization of scaffold design found these platforms to be suitable at 90 % overall porosity for particulate ranges from 100 μm and up. PDMS scaffold can be coated with adherent cells, following adsorption of fibronectin. The low endotoxin content and high biocompatibility of these PDMS scaffolds makes them appropriate for *in vivo* implantation. They can function as platforms that are conducive to tailoring to various particulate sizes, via variations in salt crystals, as well as surface properties, via protein coatings, to permit ease in application to a wide range of tissue engineered implants. While PDMS is an established material for medical implantation, its application as a macroporous scaffold via this technique is unprecedented. Therefore, we believe this represents a novel scaffold for housing cellular transplants *in vivo*.

Acknowledgements

This research was supported by the Juvenile Diabetes Research Center for Islet Transplantation at the University of Miami – Diabetes Research Institute (4-2004-361), the Diabetes Research Institute Foundation (www.diabetesresearch.org), the Department of Defense Somatic Cell Processing Facility at the DRI (N00244-07-C-1529), and Converge Biotech, Inc. E.P was supported by an NIH NIDDK Predoctoral Fellowship (1F311EB008970-01A1). We thank Dr. Luca Inverardi for his generous donation of human mesenchymal stem cells. We thank the Joanne C. and Edward A. Dauer Field-Emission Environmental Scanning Electron Microscope Laboratory for use of their instrument, in particular Dr. Edward Dauer and Ximena Vial for their technical assistance. We thank the Diabetes Research Institute Analytical Imaging Core for use of their facilities, as well as the assistance of George McNamara in image collection and processing. We thank Kevin Johnson from the Diabetes Research Institute Histology Core for his excellent skill in processing the challenging histological samples.

References

1. Bezuidenhout D, Davies N, Zilla P. Effect of well defined dodecahedral porosity on inflammation and angiogenesis. *Asaio J.* 2002; 48:465–471. [PubMed: 12296563]
2. Vacanti JP, Morse MA, Saltzman WM, Domb AJ, Perez-Atayde A, Langer R. Selective cell transplantation using bioabsorbable artificial polymers as matrices. *Journal of Pediatric Surgery.* 1988; 23:3–9. [PubMed: 2895175]
3. Mooney DJ, Mazzoni CL, Breuer C, McNamara K, Hern D, Vacanti JP, Langer R. Stabilized polyglycolic acid fibre-based tubes for tissue engineering. *Biomaterials.* 1996; 17:115–124. [PubMed: 8624388]
4. Freed LE, Vunjak-Novakovic G, Biron RJ, Eagles DB, Lesnoy DC, Barlow SK, Langer R. Biodegradable Polymer Scaffolds for Tissue Engineering. *Nat Biotech.* 1994; 12:689–693.
5. Agrawal CM, Ray RB. Biodegradable polymeric scaffolds for musculoskeletal tissue engineering. *Journal of biomedical materials research.* 2001; 55:141–150. [PubMed: 11255165]
6. Kim B-S, Mooney DJ. Development of biocompatible synthetic extracellular matrices for tissue engineering. *Trends Biotechnol.* 1998; 16:224–230. [PubMed: 9621462]
7. Ratner BD, Bryant SJ. Biomaterials: where we have been and where we are going. *Annual Review of Biomedical Engineering.* 2004; 6:41–75.
8. Sachlos E, Czernuszka JT, Road P. Making tissue engineering scaffolds work. Review on the application of solid freeform fabrication technology to the production of tissue engineering scaffolds. *Tissue Engineering.* 2003; 5:29–40.
9. Jo S, Shin H, Shung AK, Fisher JP, Mikos AG. Synthesis and characterization of oligo(poly(ethylene glycol) fumarate) macromer. *Macromolecules.* 2001; 34:2839–2844.
10. Temenoff JS, Steinbis ES, Mikos AG. Effect of drying history on swelling properties and cell attachment to oligo(poly(ethylene glycol) fumarate) hydrogels for guided tissue regeneration applications. *Journal of Biomaterials science. Polymer Edition.* 2003; 14:989–1004. [PubMed: 14661875]
11. Blomeier H, Zhang X, Rives C, Brissova M, Hughes E, Baker M, Powers AC, Kaufman DB, Shea LD, Lowe WL Jr. Polymer scaffolds as synthetic microenvironments for extrahepatic islet transplantation. *Transplantation.* 2006; 82:452–459. [PubMed: 16926587]
12. Dufour JM, Rajotte RV, Zimmerman M, Rezanian A, Kin T, Dixon DE, Korbitt GS. Development of an ectopic site for islet transplantation, using biodegradable scaffolds. *Tissue Eng.* 2005; 11:1323–1331. [PubMed: 16259588]
13. Silva A, de Matos A, Brons I, Mateus M. An overview on the development of a bio-artificial pancreas as a treatment of insulin-dependent diabetes mellitus. *Med Res Rev.* 2006; 26:181–222. [PubMed: 16342061]
14. Hayashi T. Biodegradable polymer for biomedical use. *Prog. Polymer Science.* 1994; 19:663–702.
15. Ju YM, Yu B, West L, Moussy Y, Moussy F. A novel porous collagen scaffold around an implantable biosensor for improving biocompatibility. II. Long-term in vitro/in vivo sensitivity characteristics of sensors with NDGA- or GA-crosslinked collagen scaffolds. *J Biomed Mater Res A.* 2010; 92:650–658. [PubMed: 19235209]

16. Grenier S, Sandig M, Holdsworth DW, Mequanint K. Interactions of coronary artery smooth muscle cells with 3D porous polyurethane scaffolds. *J Biomed Mater Res A*. 2009; 89:293–303. [PubMed: 18431771]
17. Scholten PM, Ng KW, Joh K, Serino LP, Warren RF, Torzilli PA, Maher SA. A semi-degradable composite scaffold for articular cartilage defects. *J Biomed Mater Res A*. 2011
18. Pedraza E, Brady A, Fraker C, Molano R, Sukert S, Kenyon N, Pileggi A, Ricordi C, Stabler C. Macro-porous PDMS Scaffolds for Extrahepatic Islet Transplantation. *Cell Transplant*. 2012 in press.
19. Aucoin L, Griffith CM, Pleizier G, Deslandes Y, Sheardown H. Interactions of corneal epithelial cells and surfaces modified with cell adhesion peptide combinations. *J Biomater Sci Polym Ed*. 2002; 13:447–462. [PubMed: 12160303]
20. Bucholz RW, Carlton A, Holmes RE. Hydroxyapatite and tricalcium phosphate bone graft substitutes. *Orthop Clin North Am*. 1987; 18:323–334. [PubMed: 3561978]
21. Heise U, Osborn JF, Duwe F. Hydroxyapatite ceramic as a bone substitute. *Int Orthop*. 1990; 14:329–38. [PubMed: 2177732]
22. Hodgins D, Wasikiewicz JM, Grahn MF, Paul D, Roohpour N, Vadgama P, Silmon AM, Cousins B, Verdon B. Biocompatible materials developments for new medical implants. *Med Device Technol*. 2007; 18:32–35. 30. [PubMed: 17939369]
23. Khorasani MT, Mirzadeh H. Laser surface modification of silicone rubber to reduce platelet adhesion in vitro. *J Biomater Sci Polym Ed*. 2004; 15:59–72. [PubMed: 15027843]
24. Nunes CR, Simske SJ, Sachdeva R, Wolford LM. Long-term ingrowth and apposition of porous hydroxylapatite implants. *J Biomed Mater Res*. 1997; 36:560–563. [PubMed: 9294773]
25. Teixeira S, Ferraz MP, Monteiro FJ. Biocompatibility of highly macroporous ceramic scaffolds: cell adhesion and morphology studies. *Journal of materials science. Materials in medicine*. 2008; 19:855–859. [PubMed: 17665126]
26. Cox ME, Dunn B. Oxygen diffusion in poly(dimethyl siloxane) using fluorescence quenching. I. Measurement technique and analysis. *J Poly Sci A: Poly Chem*. 1986; 24:621–636.
27. Merkel T, Bondar V, Nagai K, Freeman B, Pinnau I. Gas sorption, diffusion, and permeation in poly (dimethylsiloxane). *Journal of Polymer Science Part B: Polymer Physics*. 2000; 38:415–434.
28. Vollmer AP, Probst RF, Gilbert R, Thorsen T. Development of an integrated microfluidic platform for dynamic oxygen sensing and delivery in a flowing medium. *Lab on a Chip*. 2005; 5:1059–1066. [PubMed: 16175261]
29. Mata A, Fleischman A, Roy S. Characterization of Polydimethylsiloxane (PDMS) Properties for Biomedical Micro/Nanosystems. *Biomed Microdev*. 2005; 7:281–293.
30. Nishikawa M, Yamamoto T, Kojima N, Kikuo K, Fujii T, Sakai Y. Stable immobilization of rat hepatocytes as hemispheroids onto collagen-conjugated poly-dimethylsiloxane (PDMS) surfaces: Importance of direct oxygenation through PDMS for both formation and function. *Biotech Bioeng*. 2008; 99:1472–1481.
31. Toworfe GK, Composto RJ, Adams CS, Shapiro IM, Ducheyne P. Fibronectin adsorption on surface-activated poly(dimethylsiloxane) and its effect on cellular function. *Biomed Mater Res A*. 2004; 71A:449–461.
32. Brown XQ, Ookawa K, Wong JY. Evaluation of polydimethylsiloxane scaffolds with physiologically-relevant elastic moduli: interplay of substrate mechanics and surface chemistry effects on vascular smooth muscle cell response. *Biomaterials*. 2005; 26:3123–3129. [PubMed: 15603807]
33. Hillborg H, Ankner JF, Gedde UW, Smith GD, Yasuda HK, Wikstro K. Crosslinked polydimethylsiloxane exposed to oxygen plasma studied by neutron reflectometry and other surface specific techniques. *Polymer*. 2000; 41:6851–6863.
34. Li B, Chen J, Wang JH-C. RGD peptide-conjugated poly(dimethylsiloxane) promotes adhesion, proliferation, and collagen secretion of human fibroblasts. *Journal of Biomedical Materials Research Part A*. 2006; 79:989–998. [PubMed: 16948145]
35. Shiku H, Saito T, Wu CC, Yasukawa T, Yokoo M, Abe H, Matsue T, Yamada H. Oxygen permeability of surface-modified poly(dimethylsiloxane) characterized by scanning electrochemical microscopy. *Chemistry Letters*. 2006; 35:234–235.

36. Song Y, Margolles-Clark E, Fraker C, Weaver JD, Ricordi C, Pileggi A, Stabler C, Buchwald P. Feasibility of Localized Immunosuppression: 3. Preliminary Evaluation of Organosilicone Constructs Designed for Sustained Drug Release in a Cell Transplant Environment Using Dexamethasone. *Pharmazie*. 2012; 67:502–515.
37. Pedraza E, Coronel M, Fraker C, Ricordi C, Stabler C. Enhancing Beta-Cell Viability via Hydrolytically Activated, Oxygen Generating Biomaterials. *Proceedings of the National Academy of Sciences of the United States of America*. 2012; 109:4245–4250. [PubMed: 22371586]
38. Colton CK, Avgoustiniatos ES. Bioengineering in development of the hybrid artificial pancreas. *Journal of Biomechanical Engineering*. 1991; 113:152–170. [PubMed: 1875688]
39. Norman JJ, Desai TA. Control of cellular organization in three dimensions using a microfabricated polydimethylsiloxane-collagen composite tissue scaffold. *Tissue Engineering*. 2005; 11:378–386. [PubMed: 15871668]
40. Miller KM, Rose-Caprara V, Anderson JM. Generation of IL1-like activity in response to biomedical polymer implants: A comparison of in vitro and in vivo models. *Journal of biomedical materials research*. 1989; 23:1007–1026. [PubMed: 2528548]
41. Anderson JM, Ziats NP, Azeez A, Brunstedt MR, Stack S, Bonfield TL. Protein adsorption and macrophage activation on polydimethylsiloxane and silicone rubber. *Journal of Biomaterials Science, Polymer Edition*. 1996; 7:159–169. [PubMed: 7654630]
42. Karunakaran R, Kennedy JP. Synthesis, characterization, and crosslinking of methacrylate-telechelic PDMAAm-b-PDMS-b-PDMAAm copolymers. *J Poly Sci A Poly Chem*. 2007; 45:4284–4290.
43. Martin DJ, Warren LAP, Gunatillake PA, McCarthy SJ, Meijs GF, Schindhelm K. Polydimethylsiloxane / polyether-mixed macrodiol-based polyurethane elastomers : biostability. *Biomaterials*. 2000; 21:1021–1029. [PubMed: 10768754]
44. Simmons A, Hyvarinen J, Odell RA, Martin DJ, Gunatillake PA, Noble KR, Poole-Warren LA. Long-term in vivo biostability of poly (dimethylsiloxane)/poly (hexamethylene oxide) mixed macrodiol-based polyurethane elastomers. *Biomaterials*. 2004; 25:4887–4900. [PubMed: 15109849]
45. Anderson JM, Ziats NP, Azeez A, Brunstedt MR, Stack S, Bonfield TL. Protein adsorption and macrophage activation on polydimethylsiloxane and silicone rubber. *Journal of biomaterials science Polymer edition*. 1995; 7:159–169. [PubMed: 7654630]
46. Park JH, Bae YH. Hydrogels based on poly(ethylene oxide) and poly(tetramethylene oxide) or poly(dimethyl siloxane): synthesis, characterization, in vitro protein adsorption and platelet adhesion. *Biomaterials*. 2002; 23:1797–1808. [PubMed: 11950050]
47. Naim JO, van Oss CJ, Ippolito KML, Zhang J-W, Jin L-P, Fortuna R, Buehner NA. In vitro activation of human monocytes by silicones. *Colloids and Surfaces B: Biointerfaces*. 1998; 11:79–86.
48. Ely DL, Salisbury R, Hadi D, Turner M, Johnson ML. Androgen receptor and the testes influence hypertension in a hybrid rat model. *Hypertension*. 1991; 17:1104–1110. [PubMed: 2045156]
49. Jewrajka SK, Erdodi G, Kennedy JP, Ely D, Dunphy G, Boehme S, Popescu F. Novel biostable and biocompatible amphiphilic membranes. *Journal of biomedical materials research. Part A*. 2008; 87:69–77. [PubMed: 18085659]
50. Simmons A, Padsalgikar AD, Ferris LM, Poole-Warren LA. Biostability and biological performance of a PDMS-based polyurethane for controlled drug release. *Biomaterials*. 2008; 29:2987–2995. [PubMed: 18436300]

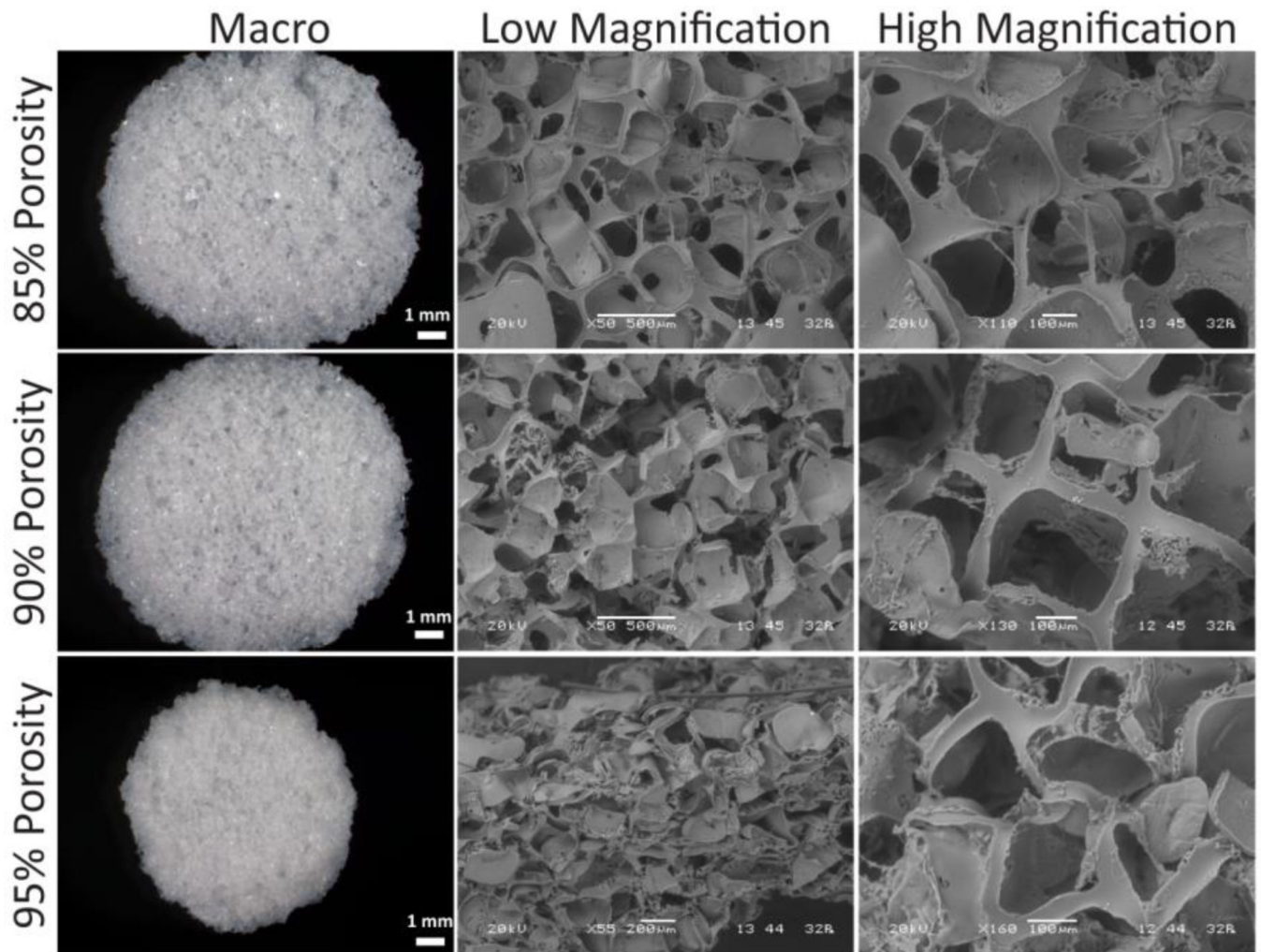


Figure 1. Photographs (left panel) and scanning electron microscope images, at low (50–55 \times , middle panel) and high magnification (110–160 \times , right panel), of 250 to 425 μm pore size scaffolds of varying porosity: 85%, 90% and 95%.

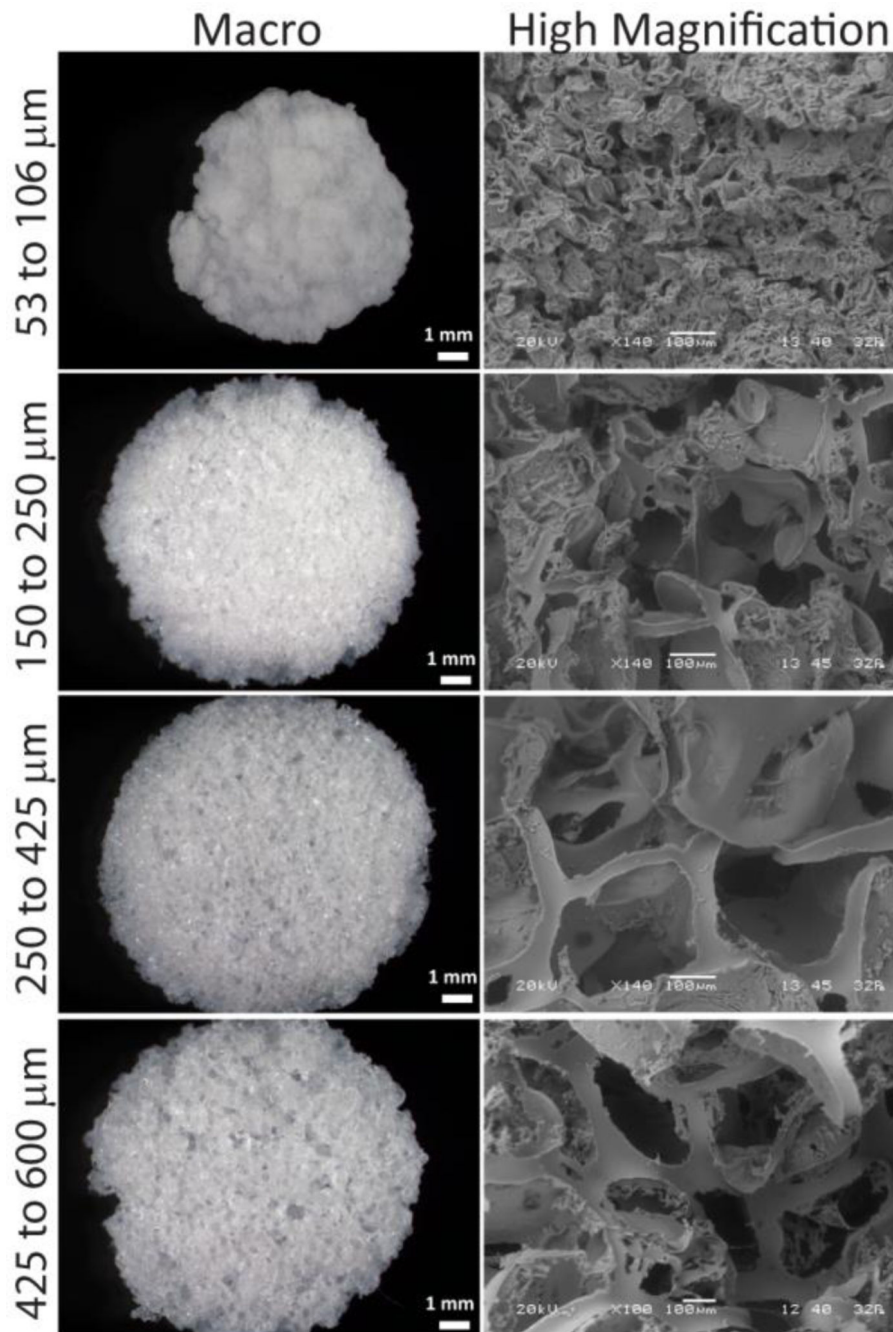


Figure 2. Photographs (left panel) and scanning electron microscope images at 100–110× magnification (right panel) of 90% porous scaffolds fabricated using salt particulates of size ranges indicated on the left.

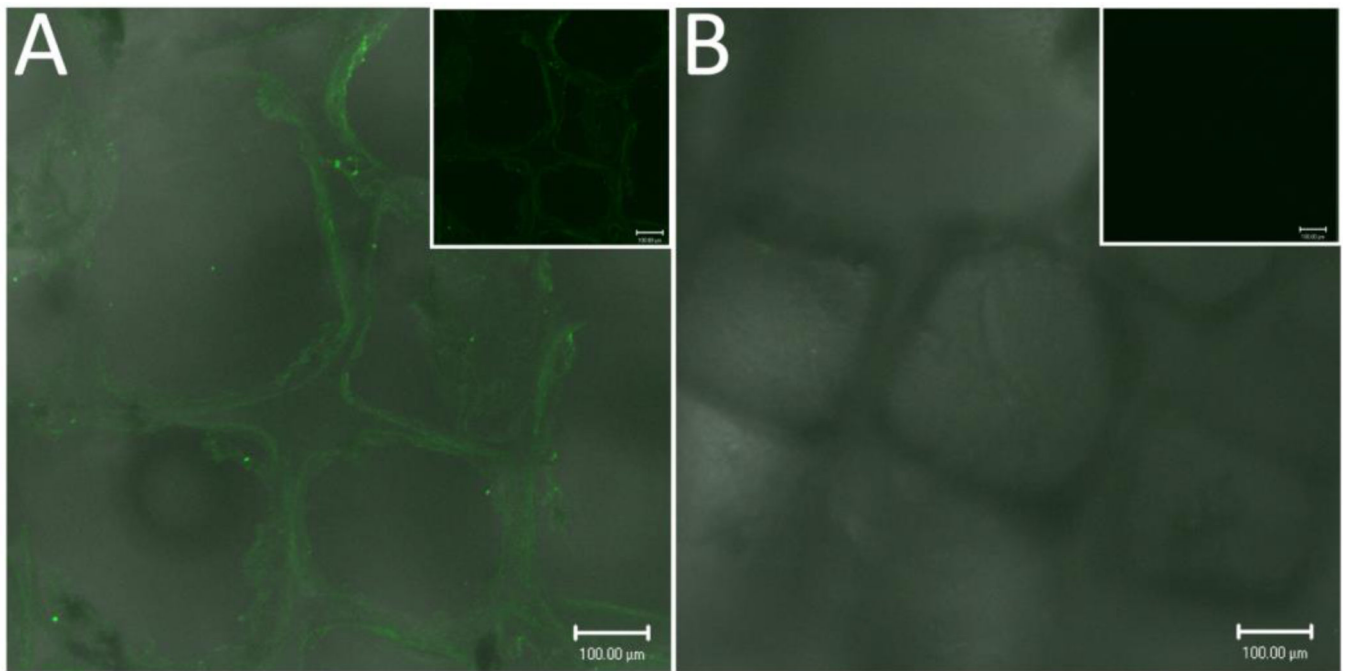


Figure 3. Confocal imaging (fluorescent/light) of fibronectin coated scaffold (A) stained with anti-fibronectin-biotin primary and streptavidin-FITC secondary antibodies, and noncoated scaffold (B). Inset: fluorescence channel only. Scale bar = 100 μm.

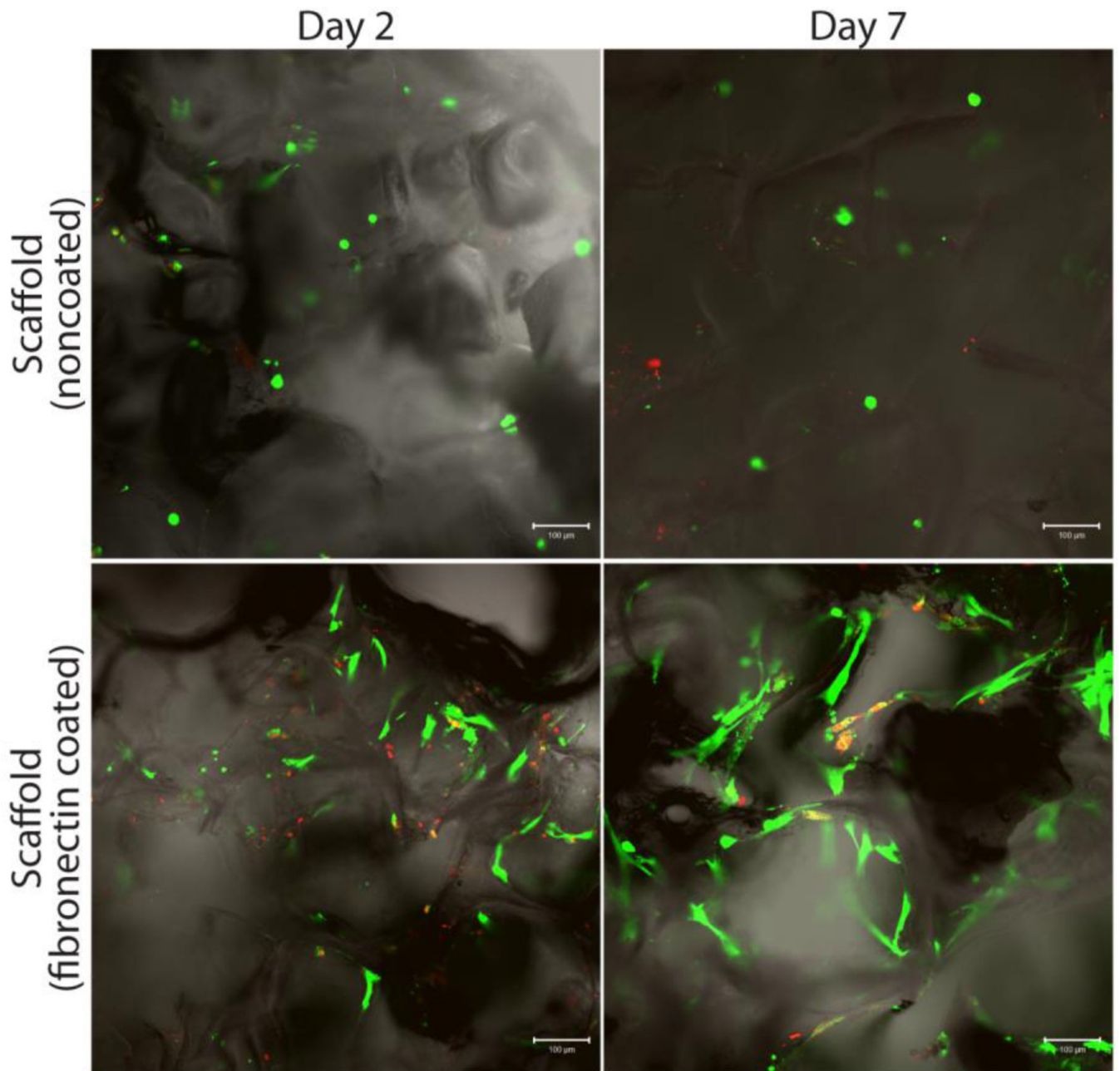


Figure 4.

Analysis of the effects of scaffold coating on cellular adhesion by visualizing live (green)/ dead (red) human MSCs growing on scaffolds. Evaluated scaffolds on days 2 (left column) and 7 (right column), respectively: untreated surface (top row) and fibronectin coated (bottom row).

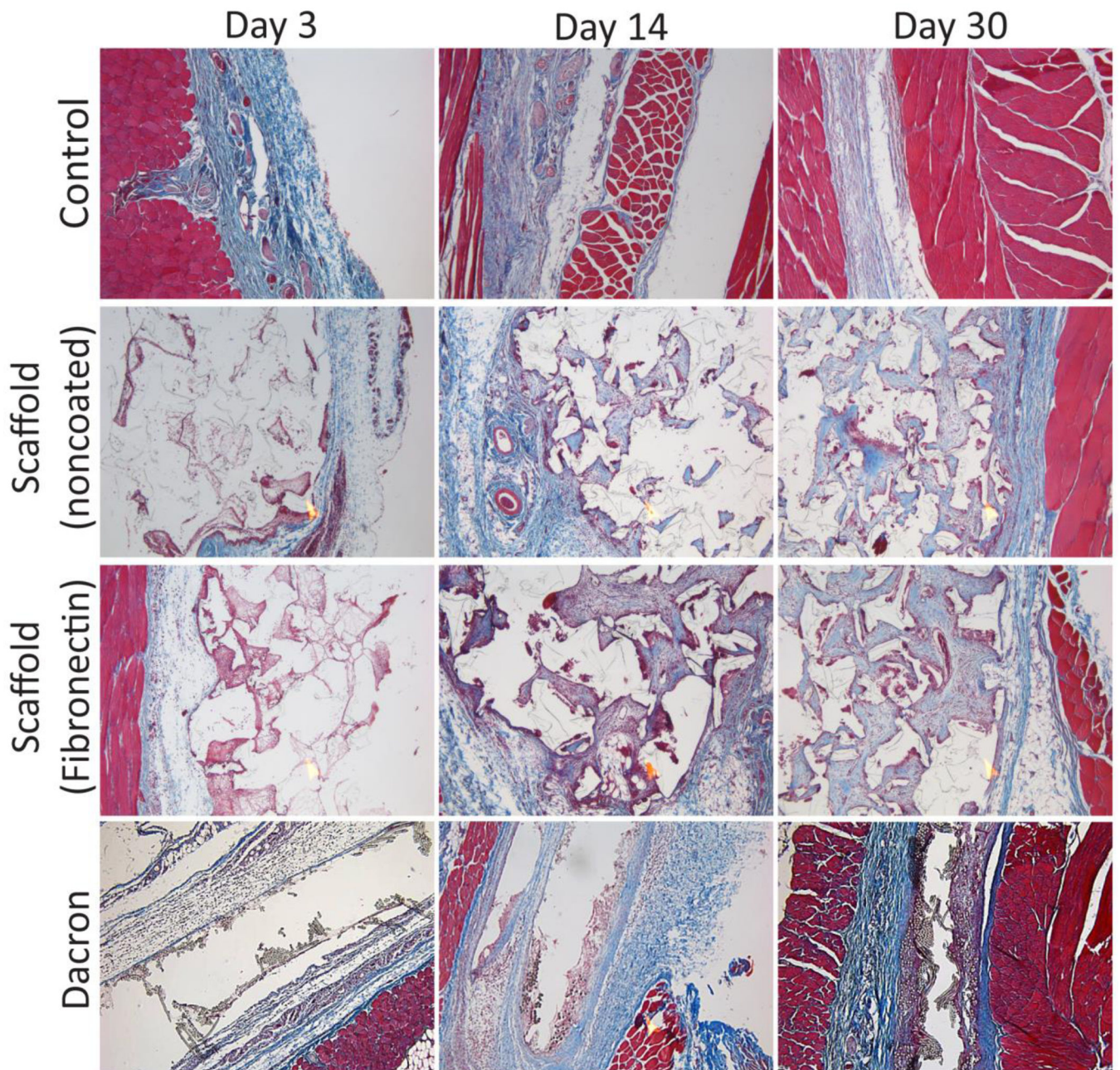


Figure 5. 5× magnification of histological cross-sections (using Masson's trichrome stain) illustrating degree of biocompatibility and potential for vascular infiltration of various biomaterials implanted into rodents.

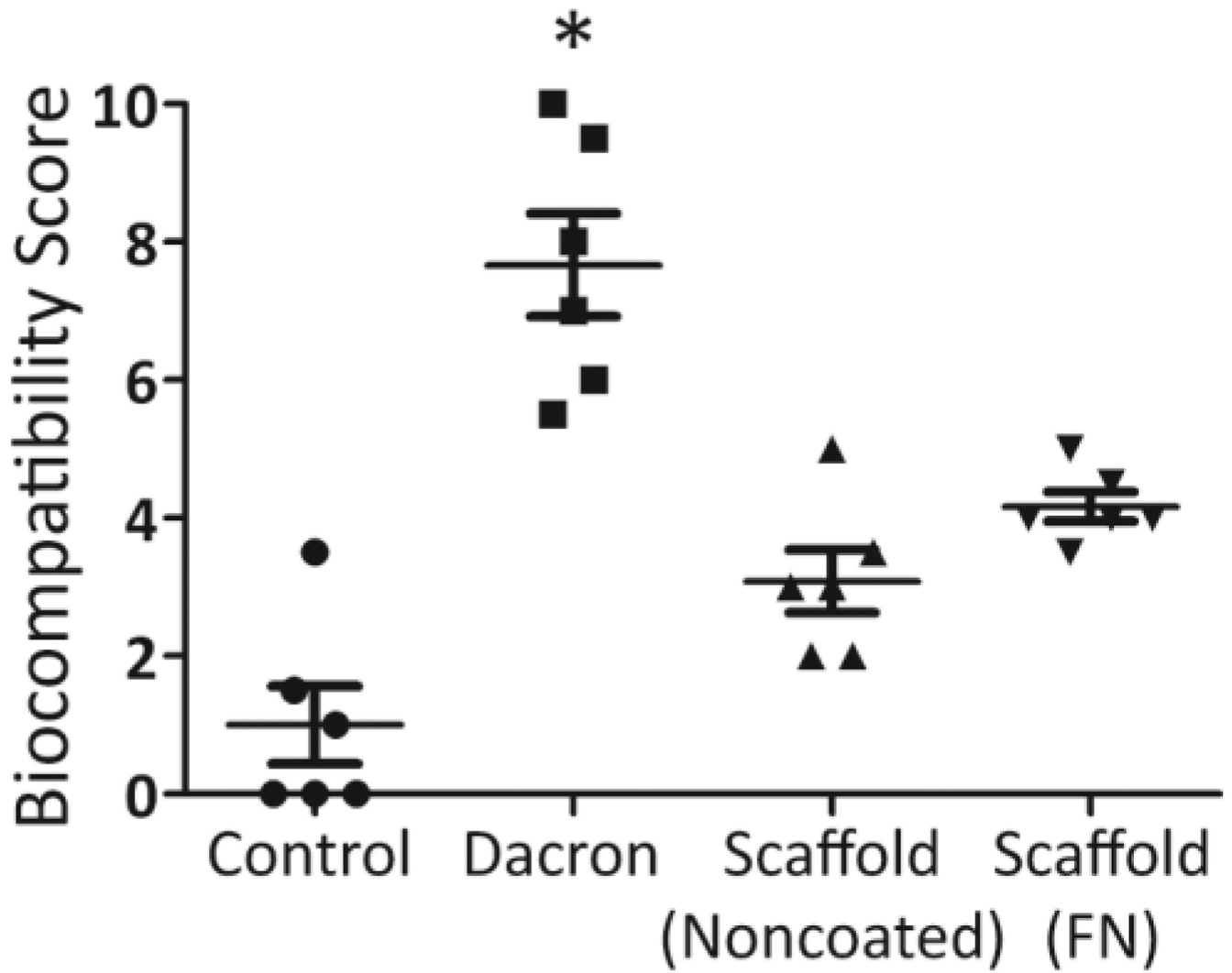


Figure 6. Biocompatibility scoring of control (no implant), Dacron, Scaffold-Noncoated, and Scaffold-FN (fibronectin coated) at day 30.* $p < 0.05$ from all other groups.

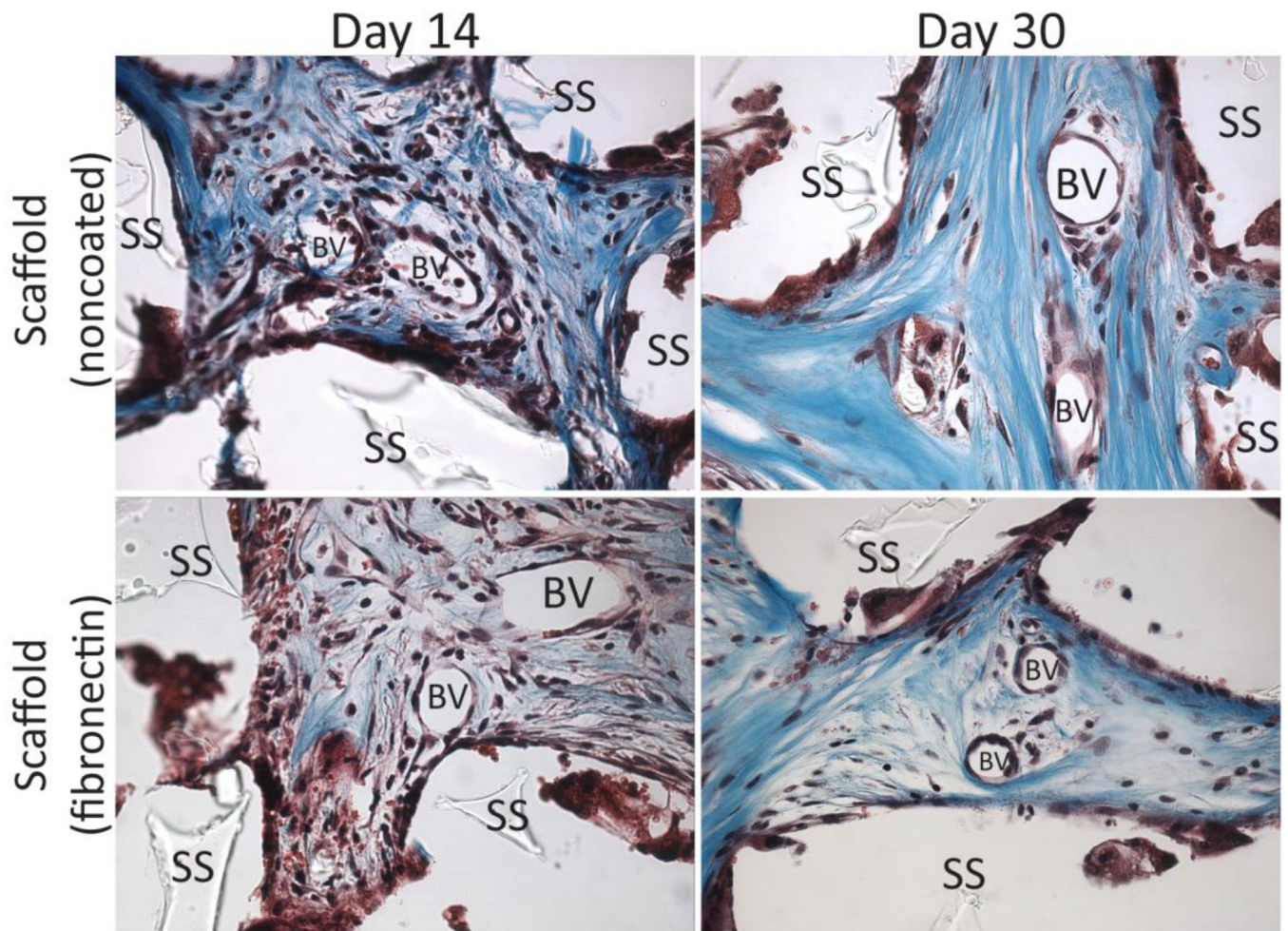


Figure 7. Identification of blood vessel (BV) infiltration into scaffolds (SS) explanted at time points indicated on histological cross-sections stained with Masson's trichrome stain.

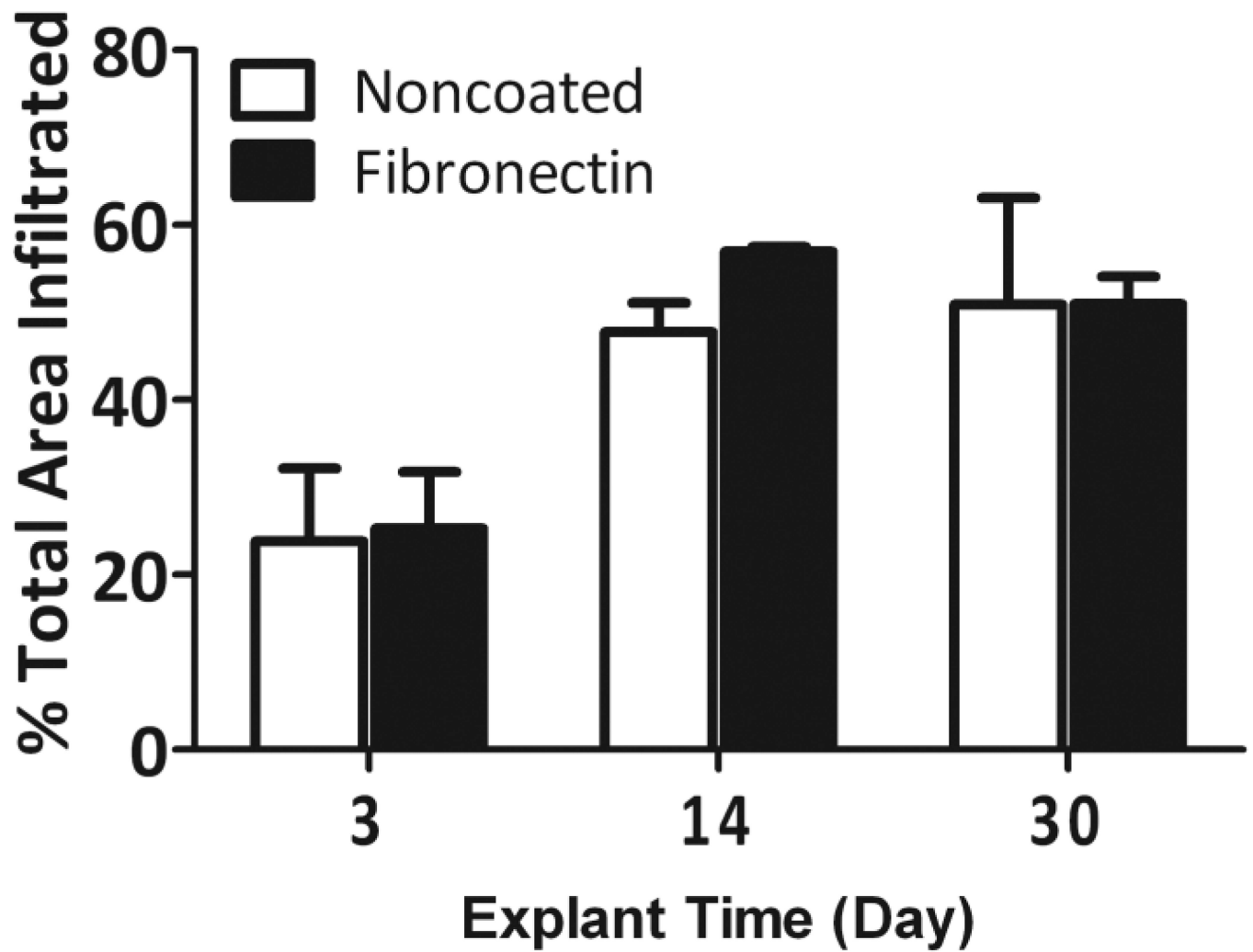


Figure 8. Total infiltration into noncoated (white bars) and fibronectin coated (black bars) scaffolds over time, as determined by Metamorph analysis as outlined in the Methods section.

Table 1
Effects of overall scaffold porosity on scaffold properties

All PDMS scaffolds were fabricated using a NaCl particulate size range from 250–425 μm . Overall porosity was varied, as indicated below. SEM was used to measure pore size and calculate pore inter-connectivity. Measured porosity was found using wet weight and dry weights, as described in the methods.

NaCl/PDMS (% vol/vol)	Final Scaffold Volume (mm^3)	Measured Pore Size (μm)	Pore Inter-connectivity, %	Measured Porosity, %
85	210 \pm 44	354 \pm 49	74 \pm 11	83 \pm 0.8
90	154 \pm 5	313 \pm 56	67 \pm 6	85 \pm 0.2
95	35 \pm 12	214 \pm 54	39 \pm 7	79 \pm 0.5
97	20 \pm 1	<i>a</i>	<i>a</i>	73 \pm 1.1

^a undetermined

Table 2
Effects of pore size on scaffold properties

All PDMS scaffolds were fabricated using 90% vol/vol NaCl/PDMS. NaCl crystal size ranges were varied, as indicated below. SEM was used to measure pore size and calculate pore inter-connectivity. Measured porosity was found using wet weight and dry weights, as described in the methods.

NaCl particulate Size Range (μm)	Final Scaffold Volume (mm^3)	Measured Pore Size (μm)	Pore Inter-connectivity, %	Measured Porosity, %
53 – 106	32 ± 6	64 ± 8	37	73 ± 0.2
150 – 250	114 ± 19	220 ± 30	67 ± 11	85 ± 0.2
250 – 425	154 ± 5	313 ± 56	67 ± 6	85 ± 0.2
425 – 600	157 ± 11	377 ± 50	74 ± 11	86 ± 0.9